

## INTRODUCTION / OVERVIEW

Characteristics and specification of the NIRx DYNOT (Dynamic Near-infrared Optical Tomography) imager:<sup>1,2</sup>

- Continuous wave (cw) Diffuse Optical Tomographic (DOT) measurements @ 2-75 fps depending of number of sources.
- Time division multiplexing of up to 32 sources (S)
- Parallel readout of up to 32 detectors (D)
- Up to four frequency-encoded wavelengths (WL)
- Dynamic detection range  $1:10^6$  (90 dB<sub>opt</sub>)
- Current applications: Mammography, imaging of peripheral vasculature, functional brain imaging, small animal imaging.

Instrumentation requirements/challenges faced in DYNOT measurements:

- Maximize number of measurement channels, to minimize the degree of underdetermined-ness of the imaging problem. Limited by practical constraints like cost, size, power consumption, etc. (DYNOT: Up to 32 S × 32 D × 4 WL = 4096 data channels)
- Data quality is critically dependent on probe placement, hardware integrity, and adequate instrument setup.
- Large number of data channels ⇒ need for automated setup and diagnostic tools
- Tissue dynamics require sampling rates of several Hz, or higher
- Long term studies (e.g., baseline studies, low frequency studies) require long term stability.

## DYNOT ARCHITECTURE AND FUNCTIONALITY

The DYNOT imaging system comprises seven layers of hardware and software integration (see Fig. 1). The three most fundamental levels are concerned with the actual instrument hardware and its control software:

### 1) Hardware:

The beams of up to four intensity modulated (3-10 kHz) laser diodes are combined and coupled into an optical switch (OS, 75-Hz switch rate), which uses a rotating mirror to sequentially redirect the light into one of up to 32 illumination fibers. The source fibers are positioned on the target with an application-specific measuring head, which also contains up to 32 fiber bundles for light collection. The latter terminate in a Programmable Multi-channel Optical Detector (PMOD), the detector channels of which are read out simultaneously in parallel. Each channel is individually digitally addressed by the host PC to assume one out of seven possible sensitivity settings. Adjusting a detector's sensitivity (its gain setting) on the fly allows accommodation of the large variation in signal strength seen by the detector during a source scan. Each detector channel contains up to four narrow-band filters (lock-in amplifiers) to electronically separate the signals emanating from the four lasers.

### 2) Software:

The most fundamental software level, which is transparent to the user, orchestrates the timing of source switching, data acquisition, and storage. Another software level is implemented in the National Instruments LabVIEW language and comprises GUI-based instrument setup, data display, and a variety of diagnostic tools. This level is the main interface through which the user interacts with the imager. Most notably, it consists of the **Setup Screen**, which allows the user to adjust the detector gain settings, a **Setup Checkout** screen, and the **Measurement Screen**, which provides real-time data display during the acquisition.

## INSTRUMENT SETUP CHECKS

The basic tasks in executing a DYNOT measurement are: 1) Placing the probes on the target site, 2) establishing detector gain settings (automated), 3) checking signal quality and possibly correcting probe / instrument setup, 4) Performance of the actual optical measurement. The first two steps crucially influence data quality: Bad probe contact promotes motion artifacts or causes coupling losses and cross-talk, thus corrupting signals, while incorrect gain settings can cause detector saturation or excessive noise. Quantitative criteria are needed to aid the user in the decision making process of whether to proceed with the measurement. Given the large number of channels, any manual approach to system checking would take too long to be practical during the measurement session. We have developed a suite of automated instrument setup check features (Fig. 1-D) that provides the user with different criteria of the integrity of the hardware setup.

### 1) Gain settings:

After the software has established the detector gains, these are visualized in a contour plot that displays all S – D combinations simultaneously, with nine color-encoded gain levels (Fig. 2-A). Each probe configuration shows a typical pattern, deviations from which are indicative of a compromised gain setup. In addition, the user can switch to a display that shows deviations in gain settings for reciprocal S – D channels, (i.e.  $S_m - D_n$  vs.  $S_n - D_m$ , see Fig. 2-B). Experience shows that deviations between reciprocal gain settings by more than one gain step is indicative of a gain setting error.

### 2) Signal levels:

A second setup check feature tests the signal levels of all S – D channels for reciprocity and displays the result in a contour plot. Displayed are color-encoded the values  $(R_{m,n} - R_{n,m}) / (R_{m,n} + R_{n,m})$  (Fig. 2-C). Excessive signal losses in either S or D channels show up as characteristic cross-patterns (see Fig. 2-C1). Optical cross talk leads to areas of increased signal asymmetry (Fig. 2-C3). Incorrect gain settings are identified by asymmetry of isolated S/D pairs (Fig. 2-C4).

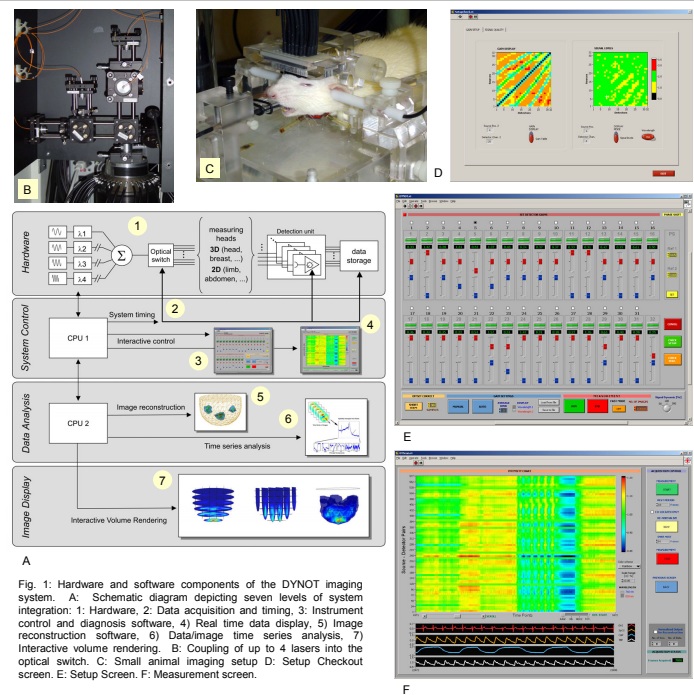


Fig. 1: Hardware and software components of the DYNOT imaging system. A: Schematic diagram depicting seven levels of system integration: 1. Hardware, 2. Data acquisition and timing, 3. Instrument control and diagnosis software, 4) Real time data display, 5) Image reconstruction software, 6) Data/image time series analysis, 7) Interactive volume rendering. B: Coupling of up to 4 lasers into the optical switch. C: Small animal imaging setup. D: Setup Checkout screen. E: Setup Screen. F: Measurement screen.

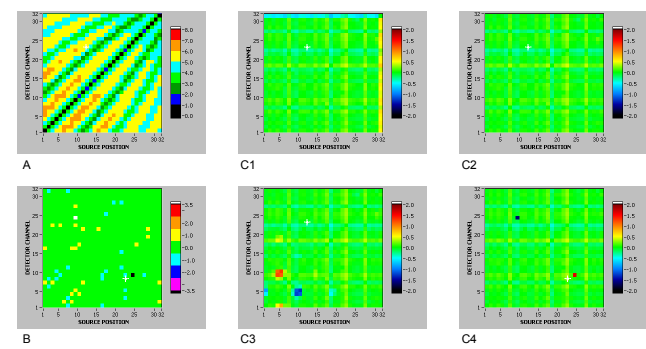


Fig. 2: System setup checks: A: Color encoded display of gain settings; notice the symmetric pattern. B: Color encoded display of differences between gain settings of reciprocal channels. Deviation by more than one step is indicative of faulty setup (as shown here for S24/D9 – S9/D24). C: Relative differences in signal level for reciprocals: C1 – bad alignment for detector fiber 31 w/ photo detector, C2 – after correcting problem seen in C1, C3 – prominent cross-talk on imaging head, C4 – faulty gain setup for S24/D9 – S9/D24 (see panel B).

## INSTRUMENT PERFORMANCE CHECKS

Several automated procedures exist to test the proper functioning of the instrument hardware components. These checks typically are performed on a regular basis, between measurement sessions. These diagnostic checks have been developed in recognition the necessity for quantitative acceptance criteria of proper functioning, and that the number of data channels renders any manual approach impractical. We will discuss the most important performance checks and show examples from a recently implemented DYNOT animal imager (32-S / 32-D / 4-WL).

### 1) Detector electronics noise/stability

An automated test exists to measure the electronic noise performance of the PMOD for the purpose of identifying deteriorating detector performance (e.g., hardware failure, component aging) or occurrence of EM interferences. The dark current is measured for each detector channel at each wavelength, depending on gain setting, and the noise values (STD) as well as the noise spectrum are displayed on-screen (Fig. 3-A). The data can be saved to the hard drive for detailed evaluation (Fig. 4). Deviation of the signal mean from zero, and changes thereof yield electronic offset and drift values (Fig. 5).

### 2) Optical / mechanical alignment

To aid in the optical alignment of four lasers with respect to the rotating mirror in the OS, a special

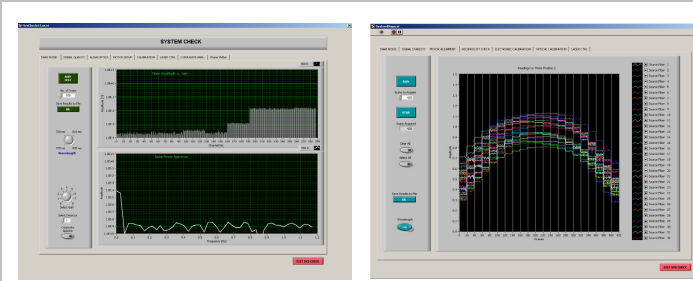


Fig. 3: Screen shots of instrument performance checks. A: Dark noise measurement establishing electronic noise level and frequency spectrum for all detector channels, at each wavelength and gain setting. B: Motor and optics alignment utility, displaying source intensity vs. position of the rotating mirror. Optimal alignment is established by judging height, center position, and width of the curve for each source channel.

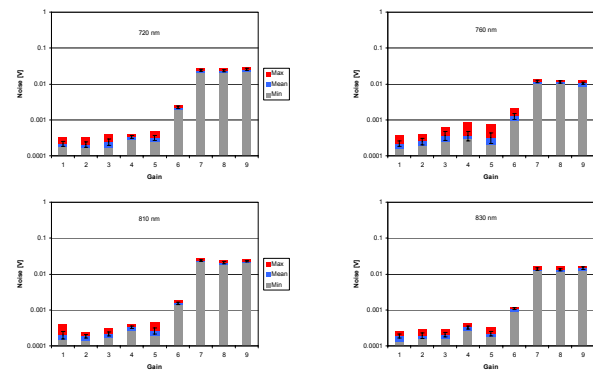


Fig. 4: Result of dark noise measurement for 4-wavelength system. The mean, the minimum, the maximum, and the standard deviation of the electronic noise values, for all detector channels at one gain setting, are depicted for each wavelength.

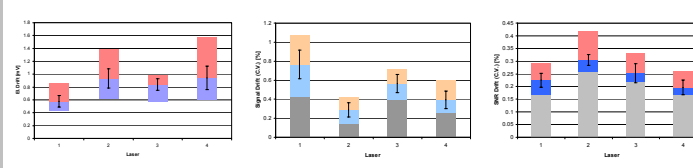


Fig. 5: Long-term offset drift of detectors. Shown for each wavelength are the mean, the minimum, the maximum, and the standard deviation of the drift of all detector channels during one hour.

### 3) Illumination noise/stability

Variation in illumination intensity is caused by variability in laser intensity as well as instabilities on part of the OS. Laser instability typically occurs as a slow drift (–s - min) and is accounted for by monitoring the laser output. The OS shows frame-to-frame variations in illumination strength due to repeatability limits of the mechanical beam-steering mechanism. In addition, thermal effects can cause long-term drift in source intensities. Both effects are measured by operating the instrument on an optical phantom in a special acquisition mode, in which only readings from the co-located S/D (i.e.,  $S_m/D_m$ ) pairs are recorded. Statistics of signal stability can then be extracted from these data to obtain noise and drift of the intensity of all sources (see Figs. 6, 7).

### 4) Instrument calibration

#### i. Optical calibration

A phantom-based calibration algorithm was implemented in the DYNOT control software, which estimates the relative illumination strengths for the different source channels and the relative sensitivities for different detector channels<sup>3</sup> (Fig. 8-A).

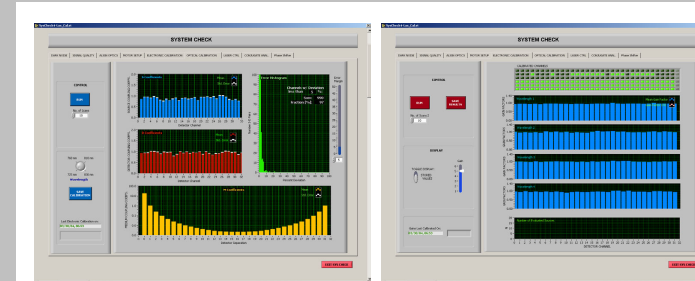


Fig. 6: Screen shots of the instrument calibration feature. A: Optical calibration screen with displays of  $d$ ,  $s$ , and  $m_i$  coefficients, as well as a histogram indicating how well the calibration model agrees with the measured results. B: Electronic calibration screen with displays of the calibration factors for wavelengths 1-4.

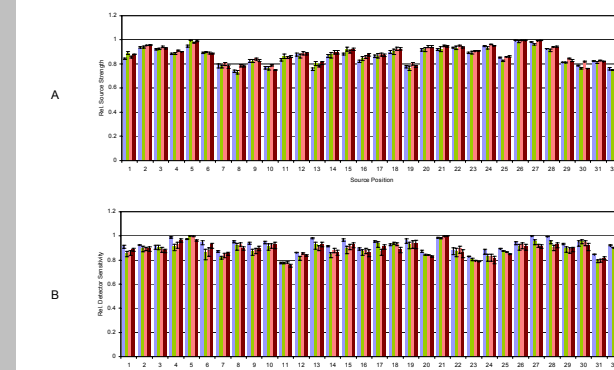


Fig. 9: Calibration results for 4-wavelength imager. A:  $s_i$  coefficients for four calibration measurements performed over the course of two days. All calibrations were performed on a Delrin cup (OD 63 mm, ID 57 mm) filled with diluted Intralipid (IL). The IL concentration was 0.5% for measurements 1-3 and 1.0% for the last measurement. Error bars indicate minimum and maximum values of the four experiments. B:  $d_i$  results for same study.

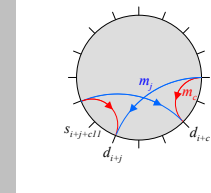


Fig. 10: Schematic illustration of the phantom-based calibration protocol as described in text. The optical signal transmitted by the phantom is assumed to depend only on the separation of S and D. According to the schematic and Eq (2), a quadruplet of readings can be used to cancel out the influence of source strengths and detector sensitivities, thus yielding estimates of  $m_{ij}$ . These estimates are used to establish relative  $s_i$  and  $d_j$  values.

The former are caused by the cumulative effect of incoupling efficiency and transmission losses for the individual source fibers, and the latter are the consequence of variations in detector fiber transmission losses, fiber – detector alignment, and component tolerances in the detection electronics. The optical calibration serves two purposes: 1) It allows for the cross-comparison of different S/D combinations, thus allowing for the estimation of the background optical properties, which cannot be gained from considering relative changes in each channel only. 2) Monitoring the calibration results readily reveals hardware deterioration in the S or the D channels of the instrument and thus adds another layer of hardware integrity check.

The algorithm is based on the premise that for a symmetric phantom, the measured light intensity for all S/D combinations are expected to depend only on S – D separation. Therefore, deviations in the readings for different S/D pairs having the same probe separation can be attributed to differences in the source strengths (expressed in source strength factors,  $0 \leq s_i \leq 1$ ) and to variations in the detector channel sensitivity (expressed in detector sensitivity factors,  $0 \leq d_i \leq 1$ ). If the fibers are placed equidistantly in one plane along the perimeter of a cylindrical phantom (see Fig. 10), the measured signals can be modeled by matrix equation (1), where  $N$  is the number of fiber locations,  $\mathbf{R}$  contains the acquired readings,  $\mathbf{M}$  represents the fraction of light transmitted from  $S_i$  to  $D_j$  by the medium, and  $\mathbf{S}$  and  $\mathbf{D}$  contain the source strength coefficients and detector sensitivity factors, respectively.

Eq. (1)

$$\mathbf{R} = \mathbf{SMD} = \begin{bmatrix} r_{11} & r_{12} & \dots & r_{1N} \\ r_{21} & r_{22} & \dots & r_{2N} \\ \vdots & \vdots & \ddots & \vdots \\ r_{N1} & r_{N2} & \dots & r_{NN} \end{bmatrix} = \begin{bmatrix} s_1 & 0 & \dots & 0 \\ 0 & s_2 & \dots & 0 \\ \vdots & \vdots & \ddots & \vdots \\ 0 & 0 & \dots & s_N \end{bmatrix} \begin{bmatrix} m_{11} & m_{12} & \dots & m_{1N} \\ m_{21} & m_{22} & \dots & m_{2N} \\ \vdots & \vdots & \ddots & \vdots \\ m_{N1} & m_{N2} & \dots & m_{NN} \end{bmatrix} \begin{bmatrix} d_1 & 0 & \dots & 0 \\ 0 & d_2 & \dots & 0 \\ \vdots & \vdots & \ddots & \vdots \\ 0 & 0 & \dots & d_N \end{bmatrix}$$

$$\Rightarrow \begin{bmatrix} r_{11} & r_{12} & \dots & r_{1N} \\ r_{21} & r_{22} & \dots & r_{2N} \\ \vdots & \vdots & \ddots & \vdots \\ r_{N1} & r_{N2} & \dots & r_{NN} \end{bmatrix} \begin{bmatrix} s_1 m_{11} d_1 & s_1 m_{12} d_2 & \dots & s_1 m_{1N} d_N \\ s_2 m_{21} d_1 & s_2 m_{22} d_2 & \dots & s_2 m_{2N} d_N \\ \vdots & \vdots & \ddots & \vdots \\ s_N m_{N1} d_1 & s_N m_{N2} d_2 & \dots & s_N m_{NN} d_N \end{bmatrix}$$

Eq. (2)

$$\frac{r_{i,j} \cdot r_{j,i} \cdot r_{i,i} \cdot r_{j,j}}{r_{i,i} \cdot r_{j,j} \cdot r_{i,i} \cdot r_{j,j}} = \frac{s_i m_{ij} d_{j,i} \cdot s_j m_{ji} d_{i,j}}{s_i m_{ii} d_{i,i} \cdot s_j m_{jj} d_{j,j}} = \frac{m_{ij}}{m_{ji}}$$

For a symmetric medium,  $\mathbf{M}$  is always a constant-diagonal (TOEPLITZ) matrix, which for a circular measurement symmetry assumes the specific form shown in Eq. (1). In this case, estimates of  $m_{ij}$  can be found by way of Eq. (2). Because the  $m_{ij}$  are normalized to an entry  $m_{ii}$  (with  $0 \leq i \leq N$  arbitrary, but fixed), the resulting matrix is a scaled version of  $\mathbf{M}$ :  $\mathbf{M}' = a \mathbf{M}$ . By creating the ratio  $r_{ij}/m'_{ij} = a s_i d_j$  and dividing each resulting element by its row sum, one obtains a number proportional to  $d_i$ :  $d'_i = m_{ii} d_i$ . Likewise, dividing elements  $a s_i d_j$  by their column sum yields estimates of the source strength coefficients  $s'_j = n s_j$ . Calibration results for the 4-WL system are shown in Fig 9.

### ii Electronic calibration

To achieve a large dynamic detection range, the DYNOT instrument uses programmable gain amplification stages that adjust the photo-electric signal of each detector channel to a level of optimal signal quality. This level is chosen to maximize the signal-to-noise ratio without risking electronic saturation while allowing proper digitization, and typically lies in the range of 100 mV – 2.0 V. Therefore, each detector reading  $r'_{ij}$  is a product of the “true” photoelectric signal  $r_{ij}$  and the gain factor  $g'_{ij}$  chosen for that specific S/D combination:  $r'_{ij} = g'_{ij} r_{ij}$ . The DYNOT amplifies the signal in nine decades,  $g'_{ij} = f_j^9 \times 10^9, f_j^1 \times 10^1, \dots, f_j^0 \times 10^0$ , where  $f_j^0 \dots f_j^9$  are calibration factors that account for deviations of the actual gains from an ideal decadic behavior. These deviations are caused by the electronic implementation of the detector gain stages. The  $f_j^k$  are specific to each detector channel and are generally close to one.

We have implemented a phantom-based calibration of the electronic gain factors, which measures the actual amplification factor between neighboring gain settings (Fig. 8-B). This is done by acquiring two sets of data, one for the optimal gain setup, and one after the detector gains are changed to the next lower or next higher setting. Care is taken to avoid signal saturation. The decrease in SNR for the second measurement is compensated for by averaging over a sequence of acquisitions. For those S/D combinations where a change in gain is feasible, the ratio of the readings is taken as an estimate of the actual gain factor between the involved gain settings. It should be noted that typically not all channels and gain settings can be calibrated in a single calibration run with one phantom. The program therefore allows merging of results of multiple calibration runs into one set of calibration factors.

The gain calibration factors are displayed and can be saved to file. They are automatically used in the optical calibration. The last date of electronic calibration is displayed, and the user is alerted if the system has not been calibrated. If an electronic calibration factor is not available, a default value of one is assumed for the optical calibration.

## REFERENCES

[1] C. H. Schmitz, M. Lacker, J. M. Lasker, A. H. Hieslacher, R. L. Barbour, “Instrumentation for fast functional optical tomography,” *Review of Scientific Instruments*, Vol. 73, pp. 429-439 (2002).  
 [2] C. H. Schmitz, H. L. Graber, R. L. Barbour, J. M. Lasker, A. H. Hieslacher, Y. Pei, “A real-time system for dynamic optical tomography,” *OSA Biomedical Topical Meetings, Advances in Optical Imaging and Motion Migration* (Miami Beach, FL, April 7-10, 2002), pp. 181-183.  
 [3] C. H. Schmitz, H. L. Graber, H. Luo, I. Arif, J. Hira, Y. Pei, A. Bluestone, S. Zhong, R. Andronica, I. Solter, N. Ramirez, S.-L. S. Barbour, R. L. Barbour, “Instrumentation and calibration protocol for imaging dynamic features in dense-scattering media by optical tomography,” *Applied Optics*, Vol. 39, pp. 6466-6486 (2000).

## ACKNOWLEDGMENTS

This work was supported by the National Institutes of Health (NIH) under Grants 1R43CA91725-1A1, R21-HL67387, R21-DK63692 and R41-CA96102, and by the US Army under Grant DAMD017-03-C-0018, and by the New York State Department of Health.